REMOTE SENSING DATA ANALYSIS FOR THE AL-AYS VOLCANIC AREA IN SOUTH WEST SAUDI ARABIA

Saad Mogren[1], Hakim Saibi[2, *], Manoj Mukhopadhyay[1], Joachim Gottsmann[3], and El-Khedr H. Ibrahim[1]

[1]Department of Geology and Geophysics, King Saud University, Riyadh, Saudi Arabia.

[2]Laboratory of Exploration Geophysics, Department of Earth Resources Engineering, Faculty of Engineering, Kyushu University, 744 Motooka, Nishi-ku, Fukuoka 819-0395, Japan.

[3] University of Bristol, Department of Earth Sciences, Bristol, UK

(* Corresponding author: E-mail address: saibi-hakim@mine.kyushu-u.ac.jp, Tel. +81-80-5268-3397, Fax. +81-92-802-3319)

Abstract

The Al-Ays Volcanic Area (AAVA) experienced a massive earthquake swarm in 2009 under the Harrat Lunayyir (HL). To examine the space distribution of basaltic lava flows in AAVA we present here an analysis of satellite images. This has helped to identify three generation of lava flows within AAVA for the first time; their spatial extent and relationship to geological features. Various remote sensing treatments were applied to the Landsat 8 image: (a) color composites, (b) band rationing, (c) principal component analysis and (d) a mathematical index. Spectral analysis of the maps assists with charting the spatial configuration of the lava flows. Total area occupied by basalts is ~ 677 km^2, of which, the oldest lava flows occupy almost 52% (354 km^2), the lavas of intermediate age share 43% (295 km^2) while the recent lava flows merely share 5% (28 km^2), including 6.8 km^2 referring to the volcanic cones. It should be noted that the generation of lava flows outlines a rather small area, of ≤ 20 km

radius, circumventing the swarm epicenter zone. These maps may prove useful in volcanic hazard mapping for the rugged terrain.

Keywords: Harrat Lunayyir; Remote sensing; Lava flows; Volcanic hazard mapping; Saudi Arabia.

1. Introduction

The Harrat Lunayyir (HL) was the site for an intense earthquake swarm of immense population in 2009 in a remote and elevated terrain in the Al-Ays. The swarm evoked much interest as there were reports on surface rupturing and dike intrusion produced by the swarm (Pallister et al. 2010). This eventually prompted the Saudi Government to evacuate nearly 30,000 residents from the nearby localities fearing volcanic eruption or an impending major earthquake. The swarm epicenter zone hit an area that is poorly geologically mapped. To pursue the investigation further, here we present an analysis on the HL volcanism based on the remote sensing data analysis. Our results are mostly complimentary to other geological and geophysical investigations for HL, however they bring out for the first time, details on (1) the episodic volcanic (flow episodes) character in the Al-Ays and their spatial extent restricted to a surprisingly small area where the 2009 swarm struck, (2) the location of the different volcanic materials.

The remote sensing data has many advantages and applications in order to study volcanic hazards due to repeated image coverage and multispectral characteristics of the data. Remote sensing data analysis has found an ever-increasing use in geosciences for more than three decades, such as: in mineral hyperspectral imaging (Azizi et al. 2015), geological mapping of rocks and structures (Saadi et al. 2008a,b; Saibi et al. 2015; Bersi et al. 2016), and also to study volcanic activity and map volcanic terrains (Francis and Baker 1978; Fedotov et al.

1989; Khrenov et al. 2000; Ramsey and Dean 2004; Ramsey and Flynn 2004). The ultraviolet (UV) remote sensing are used to study the SO_2 flux from fumaroles of volcanoes (Tamburello et al. 2011a,b,c) and also the CO_2 emissions (Aiuppa et al. 2011a,b) as precursors of volcanic eruptions. The infrared image can also help producing geological and volcanic hazard map. Of these, InSAR, is of particular usage in the evaluation and mapping of volcanic deformation (Biggs et al. 2009). In the present study, the satellite images: Band rationing and ASTER GDEM maps, aided by remote sensing interpretations is used to examine the most probable sites for magma migration and entrapment into top crust and to distinguish between the older and younger lavas in HL within AAVA. Our objectives in the present study are to present further evidence on the volcanic episodes affecting the AAVA, their respective spatial coverage in terms of total percentage volume, to focus upon the center of magmatic activity under HL in correspondence to the swarm zone epicenter, and to examine evidences for volcanic hazard estimates based on the interpretation of the remote sensing images for AAVA.

2. Study area

The AAVA occupies a surface area of about 3,575 Km^2 along the western fringe of the LIP Saudi Arabia but is somewhat isolated from the Makkah-Madinah-Nafud Volcanic Line (MMNL) (Zaidi and Mukhopadhyay 2015) (**Figure 1**). It is located close to the port-city of Umm Lajj; three most populated towns bounding the eastern periphery for the HL 2009 swarm zone are: Al-Qrash, Al-Ays and Al-Fera; these localities are identified on a shaded relief map based on remote sensing analysis. The area manifests substantial topographic relief varying from approximately 500 to 1000 m within the volcanic terrain, where a number of wadis (streams) dissects the main path leading to its elevated parts. The basement rocks belonging to two different lithostratigraphic units: Midyan terrane located to the NW and

Hijaz terrane to the SE respectively surround HL (Johnson 1998). A simplified geology map for the HL is illustrated on **Figure 2**; the epicenter zone for 2009 Al-Ays swarm is overlaid on the geology map for reference. Actual topographic relief based on remote sensing results that the spatial distribution of the volcanic cones is oriented in NW-SE direction following the direction of the Great Dikes across AAVA (**Figure 3**).

Figure 1

Figure 2

Figure 3

3. Remote sensing methodology

Landsat-8 also known as Landsat data Continuity Mission (LDCM) was designed by the National Aeronautics and Space Administration (NASA) and launched on 11 February 2013 carrying the Operational Land Imager (OLI) and the Thermal Infrared Sensor (TIRS), and subsequently transferred to USGS for routine operations (Roy et al. 2014). Placed on a sun-synchronous orbit at 705 km altitude and 10:00 a.m. equatorial crossing time for the descending node, Landsat-8 has a 16-day repeat cycle although data acquisition strategy may vary based on geographic coverage (including seasonal sampling and cloud coverage) and overall science mission objectives (Irons et al. 2012; Roy et al. 2014; Schroeder et al. 2015). The Landsat 8 multispectral images (Path: 171, Row: 43) were used to map basaltic lava flow in Harrat Lunnayir area (**Figure 4**). The image was calibrated using ENVI 5.1 and reflectance values converted to radiance values.

Treatments are applied to the multispectral content of this image as color compositing, band rationing, principal components analysis and numerical index. ASTER DEMs were used to generate shaded relief map to well map the volcanic cones.

Table 1

Figure 4

3.1. Band ratioing and ASTER GDEM for AAVA

Band ratioing is a processing method used to enhance the contrast between materials with different reflectance at specific wavelengths and conceal the topographic effects by dividing the reflectance values of a pixel in one channel by the values of the same pixel in another channel (Prost 2014). Here, we use the ratios between band5 and band4, band6 and band5 and band7 and band6, respectively, in order to discriminate between different volcanic lithologies.

3.2. Principal Components Analysis

Principal Component Analysis (PCA) is an image transformation and enhancement remote sensing technique applied to the different bands by compressing a large number of information (dimensionality reduction method) into a few principal components and overcome the correlation and redundancy using linear transformation (Li et al. 2014).

3.3. Numerical Index

In order to perform an automatic identification of specific lithologies, a mathematical operation has been used. As seen in the natural light color, basaltic flow is characterized by low reflectance value in the visible bands.

4. Results

The different band ratios band5/band4, band6/band5 and band7/band6 helped in the detection of the different volcanic units. The two basaltic units are well highlighted, the Upper Maqrah

with red color and the Lower Maqrah with purple and pink color from the Band ratioing map of HL (**Figure 5**).

Figure 5

The PCA was applied for the six (6) multispectral bands. The first three components are displayed in RGB mode (**Figure 6**).

Figure 6

Using the mathematical operation (band1+band2)/band3, the basaltic flow will be extracted with a black color and all other formations with white color (**Figure 7**).

Figure 7

Aster GDEM image and L8 images are used to map lava cones and recent lava flow. The cones form circular shapes and are well observed in both the shaded relief map and in the treated L8 image. In the band ratios (**Figure 8a**) show recent lava flow which refers to the QM5 unit which is shown with cyan color and cones are in white color. In the shaded relief map (**Figure 8b**) the cones are well highlighted with a three dimensional (3-D) aspect, we can also see the volcanic craters in the top of cones. They are illustrated by red color. The lava flow is shown with cyan color. The **Figure 8c** represents the photographic stretch map, lava flow highlighted with a dark orange color and the cones with orange color. The **Figure 8d** represents the three first PCA components displayed in RGB mode, cones appear with a light green color and the lava flow with orange color.

Figure 8

5. Discussion

Al-Amri et al. (2012) subdivided the dominant basaltic lavas at AAVA into two units based on their erosion characteristics: (a) older Tertiary unit (Jarad basalt) and (b) younger Quaternary unit (Maqrah basalt). Using natural light, it was not possible for Al-Amri et al. (2012) to differentiate between the two units. However, applying a ratio remote sensing technique we could recognize three different volcanic stages rocks belonging to the followings (**Figure 9**):

(i) The oldest lava flows with an area of 354 km^2. The natural light color composite shows the volcanic rocks with a dark color, and the surrounding area with a brown color.

(ii) The intermediate lava flows, over an area of 295 km^2.

(iii) The recent lava flows occupying a much smaller area of 29 km^2, of which, 6.78 km^2 refers to the volcanic cones.

We infer that the three groups of lavas may possibly represent three distinct stages of eruption within the AAVA; these probably owe their origin to the long-term residency of a magmatic plume and its incubation. The scenario under HL, AAVA, is different to that for recently eruptive volcanic islands in the southern Red Sea whose origin relates to episodic spreading in the Red Sea (Xu et al. 2015).

Figure 9

The HL belonging to AAVA is distinctive in several ways from the other harrats of LIP, Saudi Arabia: (a). It is offshoot from the axis of MMNL by ~100 km towards west, thus deviating from the Arabian Shield margin volcanic trend, (b). It is close to the coast (within a distance of ~20-25 km) and distinctly far away from the Tertiary Mafic Crust that is dissected by the Hizaz Escarpment; the latter is known for its fundamental importance in shaping the west margin of the Asir Igneous Province (Bohannon 1986; Mogren and Mukhopadhyay 2013); (iii) the HL is surrounded by higher and uneven topography practically on all sides; the

earthquake swarm of 2009 was localized in its central part; (iv) at least three generations of lavas are identified within the HL based on remote sensing analysis; (v) the regionally extensive Great Dikes are interrupted and largely deformed as they enter the HL, in particular, where the 2009 swarm was generated; and (vi) seismic imaging infers a low-velocity zone underneath the HL. Analysis of the remote sensing data identifies three generation of lavas, instead of two-stage lavas formally known. The HL lavas are remarkably enclosed within a small areal extent, ≤ 20 km radius. This led to the assumption that there is a long-term incubation of magma residency under the HL, probably at shallow crustal depths. This input information is considered valuable for potential field anomaly modeling under the HL – discussed elsewhere (Saibi et al. 2016).

Part of the northern 2009 earthquake swarm epicenters is close to the location of the recent basalt flow and recent volcanic cones. This observation explains that the earthquakes are related to the upward of magma through the NW-SE dykes in the form of monogenetic volcanic eruptions, which are also trending mainly in NW-SE direction.

One of the factors that influences the lava flows is ground slope, where lava moves faster on steep slopes. The slope map for HL generated from the SRTM and ADTER DEMs in a geographic information system (see **Fig. 3**) illustrates that the slopes are much steeper to the NE-SW from central part of HL but clearly are much longer as well as steeper to the SW. The steep slope extends for 20 km to NE but it is practically double of that to the SE. Furthermore, the slope direction follows the orientation of tectonic faults. This map can be used as a basis for volcanic hazard mapping as the high slope areas are considered dangerous to the lives of residents.

5. Conclusions

Band rationing and ASTER GDEM maps, aided by remote sensing interpretations for Landsat 8 image, including color composites, principal component analysis and a mathematical index, helped distinguishing between the older and younger volcanic rocks within the harrat. Three types of volcanic rocks were identified using rationing technique: oldest, intermediate and recent volcanic rocks suggesting three major flow episodes. The three groups have an area of 29 km^2, 295 km^2, and 354 km^2 respectively.

The northern group of the 2009 earthquake swarm epicenters is located near to the recent magmatic features (basalt flow and volcanic cones) detected by the Band ratioing technique, suggesting a volcanic activity in the NW-SE direction parallel to the regional dyke direction.

The remote sensing results agree in general with the geological boundaries detected from field surveys (**Figure 10**). The remote sensing shows its capabilities to cartography the surface geological and volcanological features.

Figure 10

Acknowledgments

This research was funded by the National Plan for Science, Technology and Innovation (MAARIFAH), King Abdulaziz City for Science and Technology, Kingdom of Saudi Arabia, Award Number (12-SPA2872-02)

References

Aiuppa A, Burton M, Allard P, Caltabiano T, Giudice G, Gurrieri S, Liuzzo M, Salerno G (2011a) First observational evidence for the CO2-driven origin of Stromboli's major explosions. Solid Earth 2:135-142. doi:10.5194/se-2-135-2011.

Aiuppa A, Burton M, Allard P, Caltabiano T, Giudice G, Gurrieri S, Liuzzo M, Salerno G (2011b) Linking plume CO_2 flux emissions and eruptive activity at Stromboli volcano (Italy) (abs.). In 11th gas Workshop, Kamchatka, Russia, 1-10 Sept. 2011, Commission on the Chemistry of Volcanic Gases (CCVG)-IAVCET: 6.

Al-Amri AM, Fnaism MS, Abdel-Rahman K, Mogren S, Al-Dabbagh M (2012) Geochronological dating and stratigraphic sequences of Harrat Lunayyir, NW Saudi Arabia. International Journal of Physical Sciences 7 (20):2791-2805.

Azizi M, Saibi H, Cooper GRJ (2015) Mineral and structural mapping of the Aynak-Logar Valley (Eastern Afghanistan) from hyperspectral remote sensing data and aeromagnetic data. Arabian Journal of Geosciences 8:10911-10918. doi: 10.1007/s12517-015-1993-2.

Bersi M, Saibi H, Chabou MC (2016) Aerogravity and remote sensing observations of an iron deposit in Gara Djebilet, southwestern Algeria. Journal of African Earth Sciences 116:134-150. doi: 10.1016/j.jafrearsci.2016.01.004.

Biggs J, Anthony EY, Ebinger C (2009) Multiple inflation and deflation events at Kenyan volcanoes. East African Rift. Geology 37:979-982.

Bohannon RG (1986) Tectonic configuration of the Western Arabian continental margin, Southern Red Sea. Tectonics 5(4):477-499. doi:10.1029/TC005i004p00477

Fedotov SS, Dobrynin NF, Dvigalo VN (1989) An analytical-photogrammetric system for the quantitative study of volcanic features. Mapping Sciences and Remote Sensing 26 (4):314-324.

Francis PW, Baker MCW (1978) Sources of two large volume ignimbrites in the Central Andes: some LANDSAT evidence. Journal of Volcanology and Geothermal Research 4:81-87.

Irons JR, Dwyer JL, Barsi JA (2012) The next landsat satellite: the landsat data continuity mission. Remote Sensing of Environment 112:11-21.

Johnson PR (1998) Tectonic map of Saudi Arabia and adjacent areas. Deputy Ministry for Mineral Resources Technical Report USGS-TR-98-3 (IR 948).

Khrenov AP, Pieri D, Blinkov AM, Zaytsev VV, Shkarin V Ye (2000) Monitoring of active volcanoes on Lamachtka from thermal infrared scanner and radar imagery. Mapping Sciences and Remote Sensing 37 (4):260-278.

Li C et al. (2014) Volcanic ash cloud detection from remote sensing images using principal component analysis. Computers and Electrical Engineering 40:204-214.

Mogren S, Mukhopadhyay M (2013) Gravity modeling for the rifted crust at the Arabian Shield margin – Further insight into Red Sea Spreading. Open Journal of Geology 3:28-33.

Mukhopadhyay B, Mogren S, Mukhopadhyay M, Dasgupta S (2012) Incipient status of dyke intrusion in top crust-evidences from the Al-Ays 2009 earthquake swarm, Harrat Lunayyir, SW Saudi Arabia. Geomatics Natural Hazards and Risk 1-19.

Pallister J et al. (2010) Broad accommodation of rift-related extension recorded by dyke intrusion in Saudi Arabia. Nature Geoscience 3:705-712. doi:10.1038/ngeo966

Prost GL (2014) Remote sensing for geoscientists: image analysis and integration, 3rd edition. CRC Press, Taylor & Francis Group 674 p.

Ramsey M, Dean J (2004) Spaceborne observations of the 2000 Bezymianny, Kamchatka eruption: the integration of high-resolution ASTER data into near real-time monitoring using AVHRR. Journal of Volcanology and Geothermal Research 135:127-146.

Ramsey MS, Flynn LP (2004) Strategies, insights and the recent advances in volcanic monitoring and mapping with data from NASA's Earth Observing System. Journal of Volcanology and Geothermal Research 135:1-11.

Roy D, Wulder MA, Loveland TR, Woodcock CE, Allen RG, Anderson MC, Zhu Z (2014) Landsat-8: Science and product vision for terrestrial global change research. Remote Sensing of Environment 145:154-172.

Saadi N, Aboud E, Saibi H, Watanabe K (2008a) Integrating Data from Remote Sensing, Geology and Gravity for Geological Investigation in the Tarhunah Area, Northwest Libya. International Journal of Digital Earth 1 (4):347-366.

Saadi N, Watanabe K, Imai A, Saibi H (2008b) Integrating potential fields with remotely sensed data for geological investigations in Eljufra area, Libya. Earth, Planets and Space 60 (6):539-547.

Saibi H, Azizi M, Mogren S (2015) Structural investigations of Afghanistan deduced from remote sensing and potential field data. Acta Geophysica. in press.

Saibi H, Gottsmann J, Mogren S, Mukhopadhyay M, Ibrahim E (2016) Subsurface imaging of the harrat lunayyir 2009 earthquake swarm zone, western Saudi Arabia. Paper in preparation for submission.

Schroeder W, Oliva P, Giglio L, Quayle B, Lorenz E, Morelli F (2015) Active fire detection using Landsat-8/OLI data. Remote Sensing of Environment http://dx.doi.org/10.1016/j.rse.2015.08.032.

Tamburello G, McGonigle AJS, Kantzas EP, Aiuppa A (2011b) Recent advances in ground-based ultraviolet remote sensing of volcanic SO2 fluxes. Annals of Geophysics 54 (2):199-208.

Tamburello G, Kantzas EP, McGonigle AJS, Aiuppa A, Guidice G (2011c) UV camera measurements of fumarole field degassing (La Fossa crater, Vulcano Island). Journal of Volcanology and Geothermal Research 199:47-52. doi: 10.1016/j.jvolgeores.2010.10.004.

Tamburello G, Kantzas EP, McGonigle AJS, Aiuppa A (2011a) Vulcamera: a program for measuring volcanic SO_2 using UV cameras. Annals of Geophysics 54 (2):219-221.

Xu W, Ruch J, Jonsson S (2015) Birth of two volcanic islands in the southern Red Sea. Nature Communications 6:7104. doi: 10.1038/ncomms8104.

Zaidi FK, Mukhopadhyay M (2015) Morphometric analysis of the scoria cones and drainage pattern for the Quaternary and older volcanic fields in parts of the Large Igneous Province, Saudi Arabia. Journal of African Earth Sciences 110:1-13.

Table Caption

Table 1: OLI instrument parameters (Prost, 2014).

Band	Bandwith (nm)	Resolution (m)	Swath (km)
1, Coastal/aerosol	433-453	30	185
2, Blue	450-515	30	185
3, Green	525-600	30	185
4, Red	630-680	30	185
5, NIR	845-885	30	185
6, SWIR 1	1560-1660	30	185
7, SWIR 2	2100-2300	30	185
8, PAN	500-680	15	185
9, Cirrus	1360-1390	30	185

Figures Captions

Figure 1: The Harrat Lunayyir located within the Al-Ays Volcanic area, where the 2009 earthquake swarm struck. It is a part of the Large Igneous Province in Saudi Arabia.

Figure 2: (a) Geologic outline map for the Harrat Lunayyir belonging to the Al-Ays Volcanic Area (after Mukhopadhyay et al., 2012). (b) Magnetic anomaly map of HL and its surroundings showing the Cenozoic dykes striking NW-SE.

Figure 3: Digital elevation model map for the Harrat Lunayyir belonging to the Al-Ays Volcanic Area. Slope index is in colour. Red line shows the boundary of HL.

Figure 4: The natural light color composite map for the Harrat Lunayyir showing the areal disposition of the volcanic rocks (dark color), and its surroundings (brown color).

Figure 5: Band ratioing (band5/band4, band6/band5 and band7/band6) image map for the Harrat Lunayyir. The Upper Maqrah basalt (Recent lavas) appears with blue color whereas the Lower Maqrah in purple.

Figure 6: The Principal Component Analysis applied for the 6 multispectral bands specific to the volcanics in the Al-Ays Volcanic Area. Note that the first three components are displayed in RGB mode. The two basaltic units are well highlighted; the Upper Maqrah (red color) and the Lower Maqrah (purple and pink color).

Figure 7: Numerical Index Map for the Al-Ays Volcanic Area exhibiting the extent of basaltic flows (dark color) against the backdrop of all other formations (blank areas).

Figure 8: Remote sensing results showing the more conspicuous volcanic cones and rocks: (a). Refers to the band rationing results (band5/band4, band6/band5 and band7/band6), the Volcanic Cones (VC) are in white color, (b). Consists of the shaded relief map using ASTER Global Digital Elevation Model - the VC presents a relief on Cones. The northern 2009 earthquake swarm epicenters are spatially related to the recent volcanic flows. (c). Photographic stretch map for the VC (orange color) and (d). First three components derived from the Principal Components Analysis process displayed on RGB. Note that the spatial distribution of this VC is controlled following the NW-SE direction.

Figure 9: Location map for the three examples of volcanic components present in Al-Ays Volcanic Area and corresponding spectral signature of the AAVA volcanic components.

Figure 10: Band ratioing map overlay on shaded relief map of HL. Yellow lines show the litho-geological boundaries from geological field data. Red lines show the geological structures. Black dotes represent the 2009 earthquake swarm epicenters.

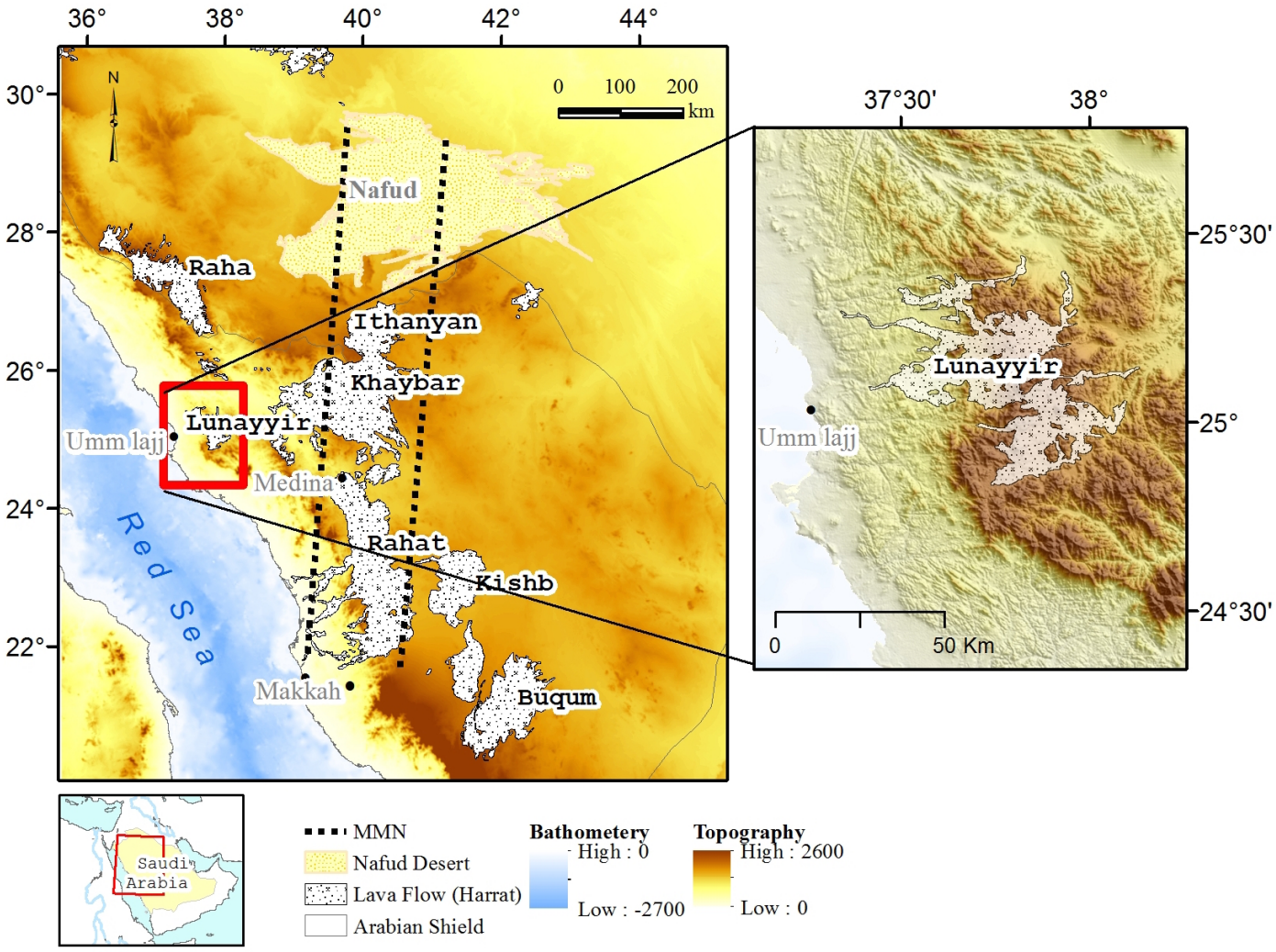
36°
38°
40°
42°
44°
30°
28°
26°
24°
22°
N
0 100 200
km
Nafud
Raha
Ithanyan
Khaybar
Lunayyir
Umm lajj
Medina
Rahat
Kishb
Red Sea
Makkah
Buqum
37°30'
38°
25°30'
25°
24°30'
Lunayyir
Umm lajj
0
50 Km
Saudi Arabia
MMN
Nafud Desert
Lava Flow (Harrat)
Arabian Shield
Bathometery
High : 0
Low : -2700
Topography
High : 2600
Low : 0

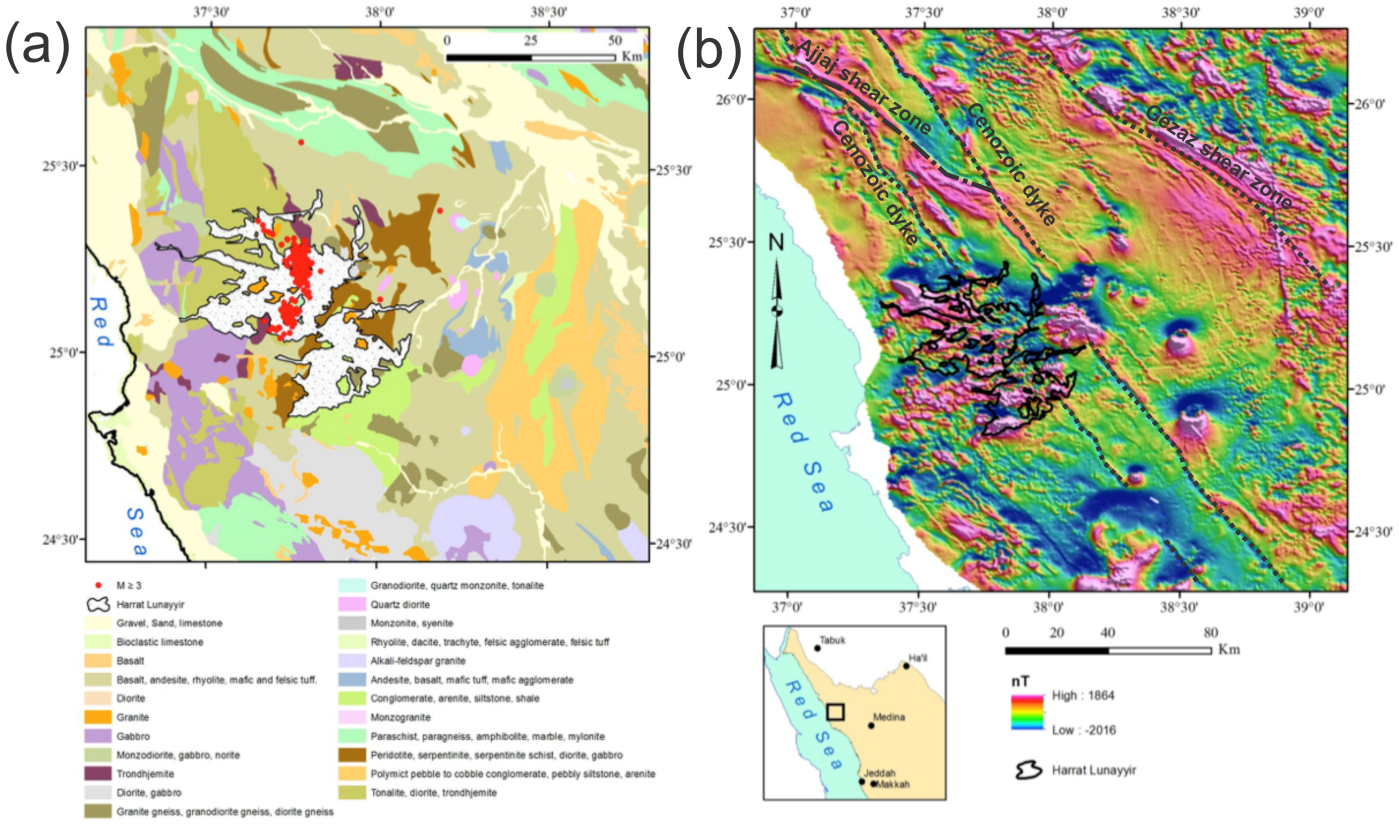
(a)
37°30'
38°0'
38°30'
0 25 50 Km
25°30'
25°0'
24°30'
Red Sea
M ≥ 3
Harrat Lunayyir
Gravel, Sand, limestone
Bioclastic limestone
Basalt
Basalt, andesite, rhyolite, mafic and felsic tuff.
Diorite
Granite
Gabbro
Monzodiorite, gabbro, norite
Trondhjemite
Diorite, gabbro
Granite gneiss, granodiorite gneiss, diorite gneiss
Granodiorite, quartz monzonite, tonalite
Quartz diorite
Monzonite, syenite
Rhyolite, dacite, trachyte, felsic agglomerate, felsic tuff
Alkali-feldspar granite
Andesite, basalt, mafic tuff, mafic agglomerate
Conglomerate, arenite, siltstone, shale
Monzogranite
Paraschist, paragneiss, amphibolite, marble, mylonite
Peridotite, serpentinite, serpentinite schist, diorite, gabbro
Polymict pebble to cobble conglomerate, pebbly siltstone, arenite
Tonalite, diorite, trondhjemite
(b)
37°0'
37°30'
38°0'
38°30'
39°0'
26°0'
25°30'
25°0'
24°30'
Ajaj shear zone
Cenozoic dyke
Cenozoic dyke
Gazal shear zone
N
Red Sea
Tabuk
Ha'il
Medina
Jeddah
Makkah
0 20 40 80 Km
nT
High : 1864
Low : -2016
Harrat Lunayyir

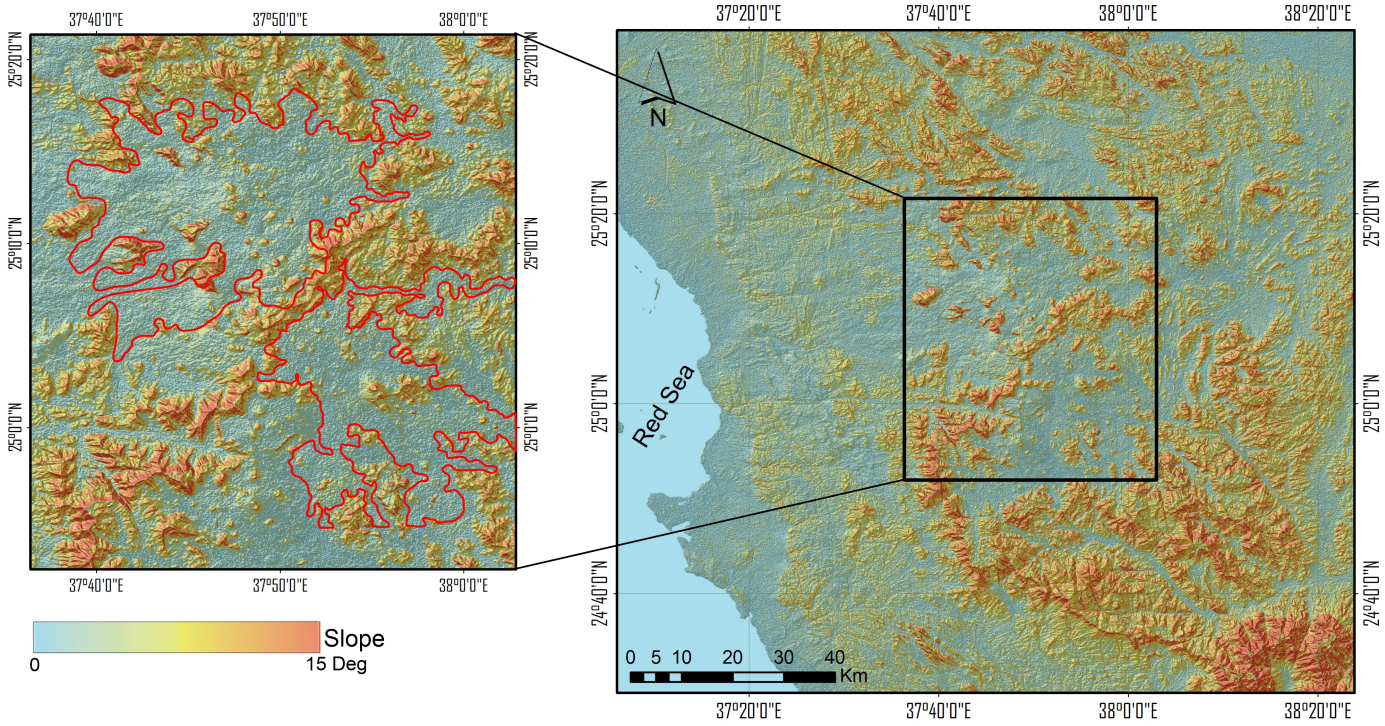
37°40'0"E
37°50'0"E
38°0'0"E
25°20'0"N
25°10'0"N
25°0'0"N
Slope
0
15 Deg
37°20'0"E
37°40'0"E
38°0'0"E
38°20'0"E
N
Red Sea
24°40'0"N
0 5 10 20 30 40
Km

37°30'0"E
37°40'0"E
37°50'0"E
38°0'0"E
38°10'0"E
25°20'0"N
25°10'0"N
25°0'0"N
24°50'0"N
N
0 3 6 12 18 24
Km

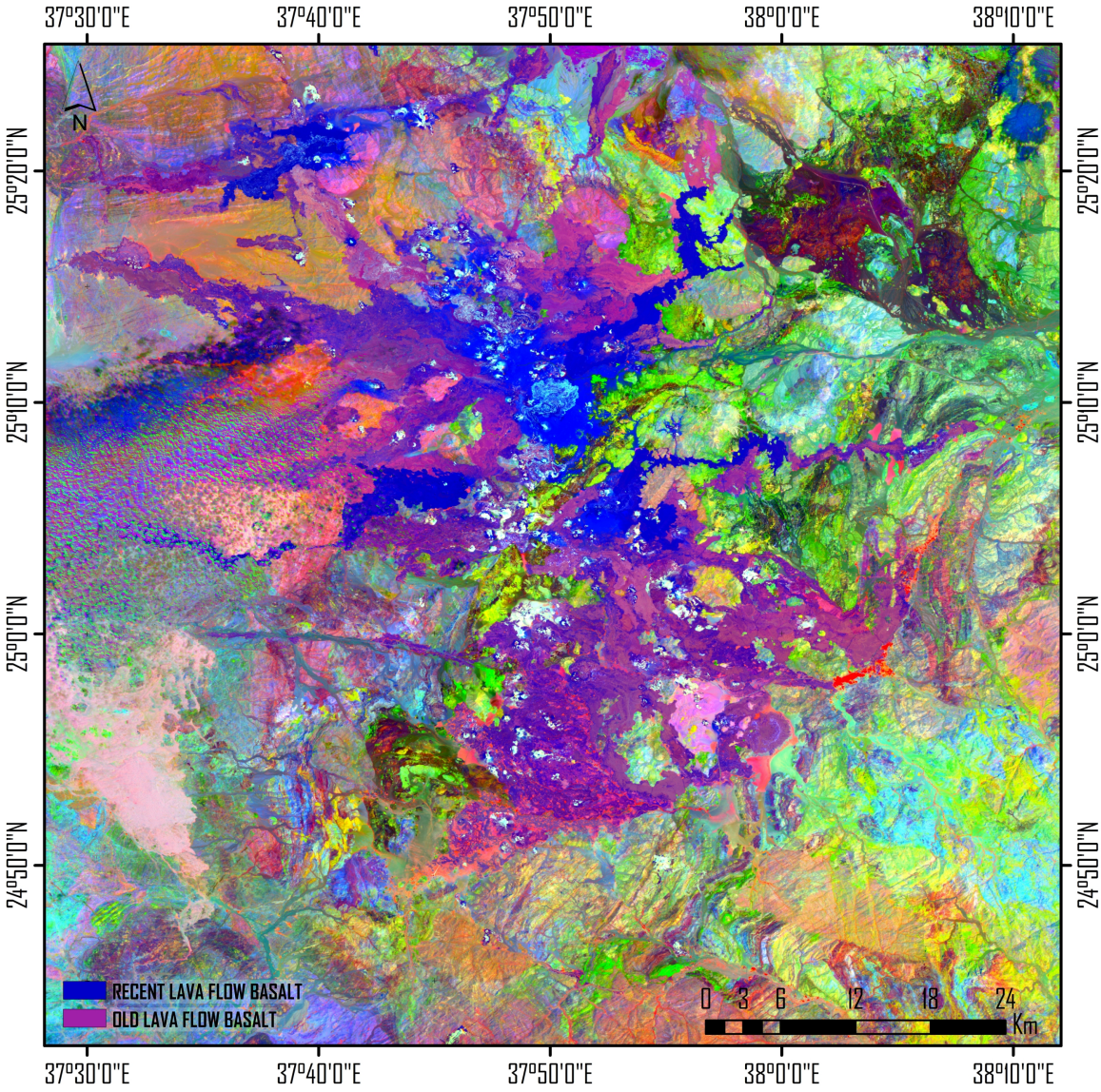
37°30'0"E
37°40'0"E
37°50'0"E
38°0'0"E
38°10'0"E
25°20'0"N
25°10'0"N
25°0'0"N
24°50'0"N
N
RECENT LAVA FLOW BASALT
OLD LAVA FLOW BASALT
0 3 6 12 18 24
Km

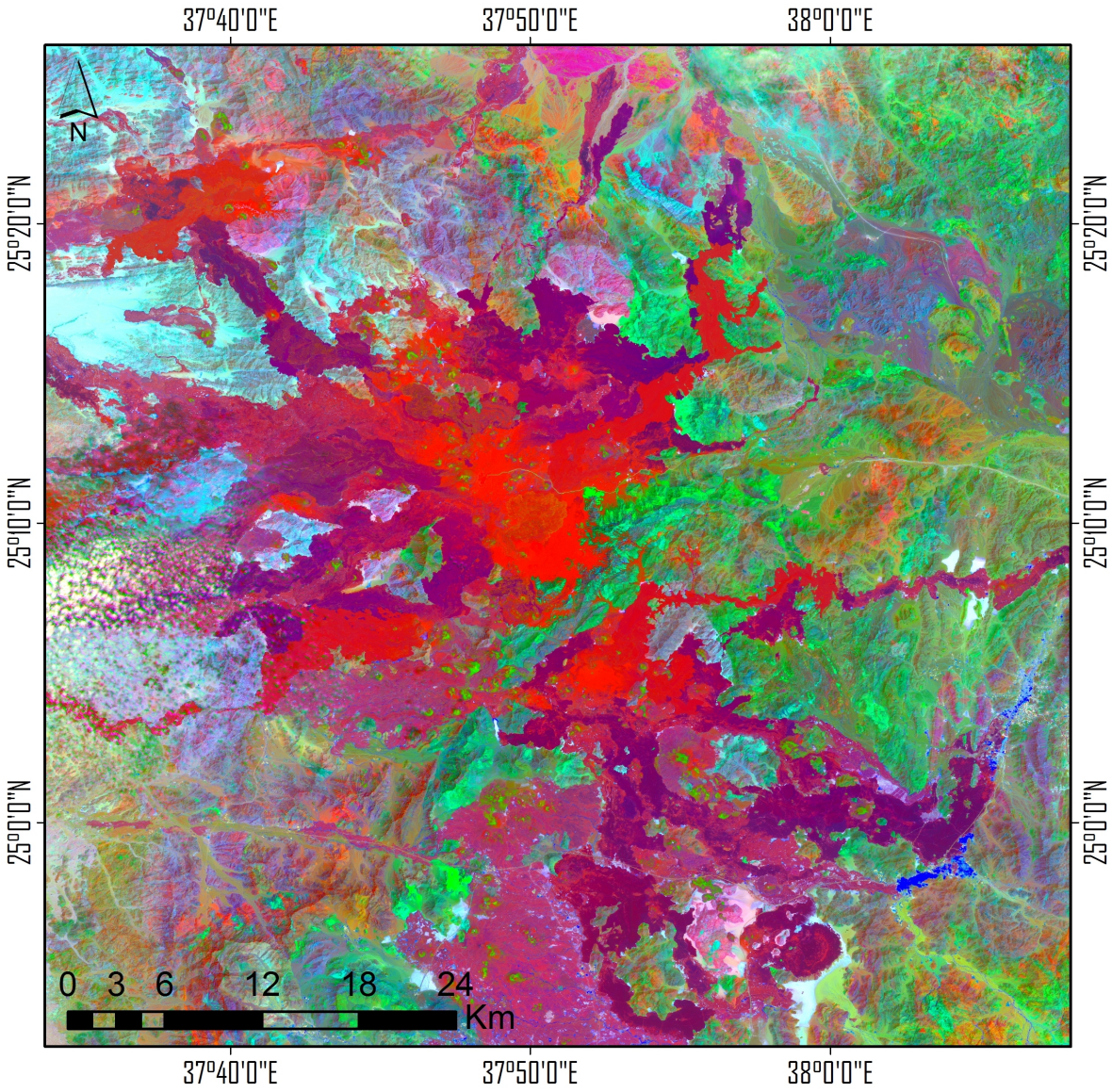
37°40'0"E
37°50'0"E
38°0'0"E
25°20'0"N
25°10'0"N
25°0'0"N
N
0 3 6 12 18 24
Km

37°30'0"E
37°40'0"E
37°50'0"E
38°0'0"E
38°10'0"E
25°20'0"N
25°10'0"N
25°0'0"N
24°50'0"N
N
0 3 6 12 18 24
Km

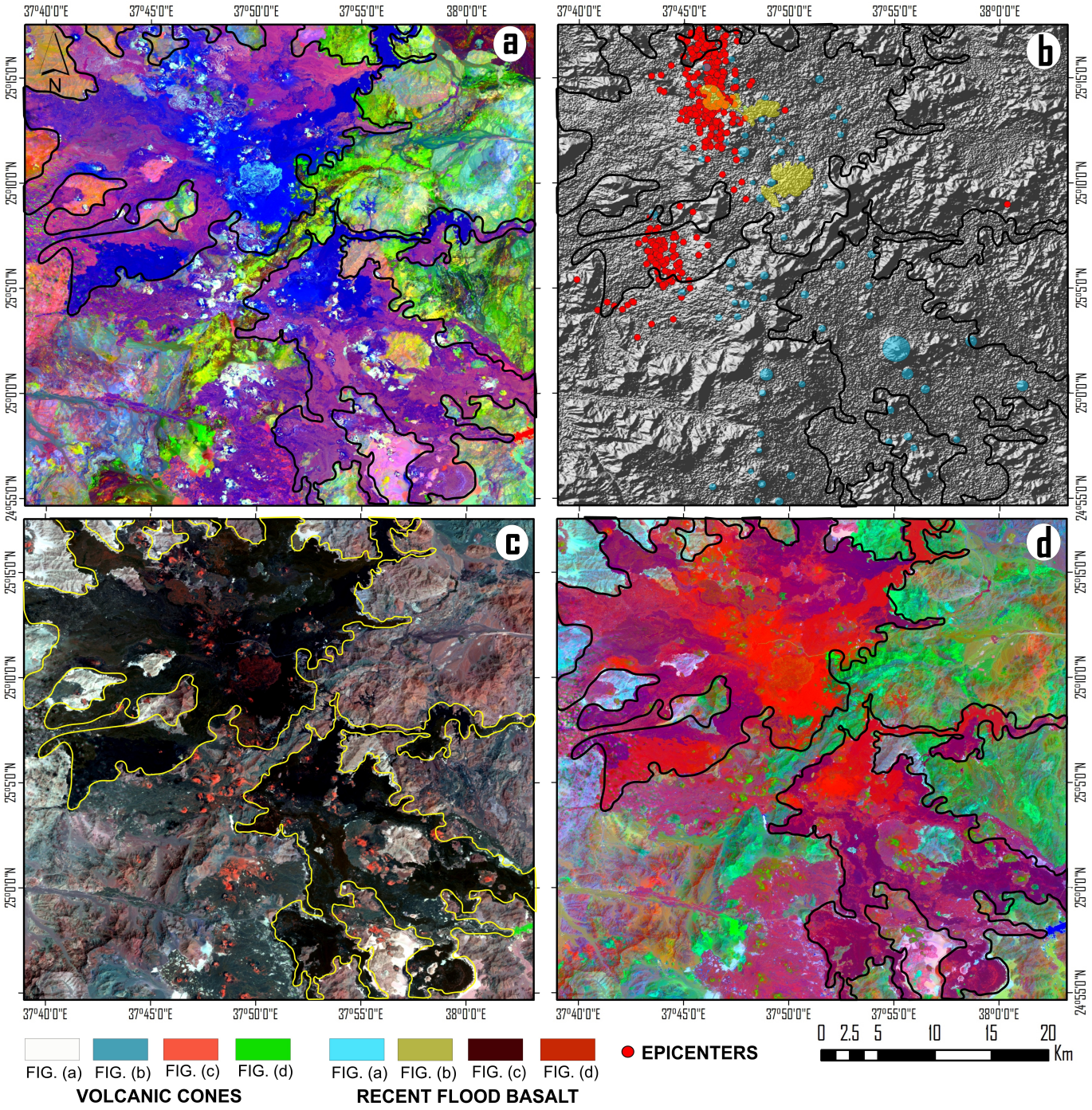
37°40'0"E
37°45'0"E
37°50'0"E
37°55'0"E
38°0'0"E
25°15'0"N
25°10'0"N
25°5'0"N
25°0'0"N
24°55'0"N
a
b
c
d
N
FIG. (a)
FIG. (b)
FIG. (c)
FIG. (d)
VOLCANIC CONES
FIG. (a)
FIG. (b)
FIG. (c)
FIG. (d)
RECENT FLOOD BASALT
EPICENTERS
0 2.5 5 10 15 20
Km

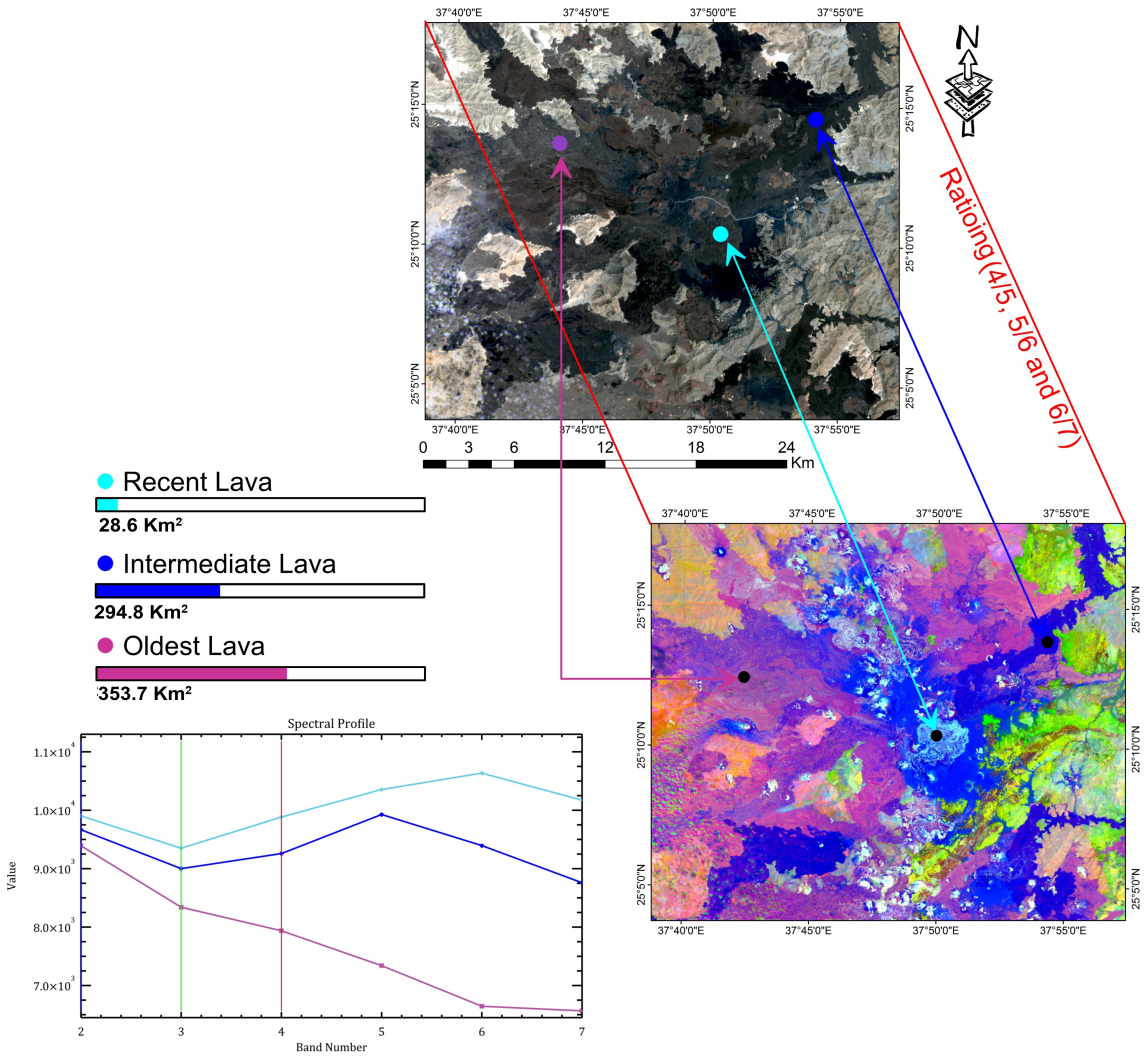
37°40'0"E
37°45'0"E
37°50'0"E
37°55'0"E
25°15'0"N
25°10'0"N
25°5'0"N
N
Ratioing(4/5, 5/6 and 6/7)
0 3 6 12 18 24
Km
Recent Lava
28.6 Km²
Intermediate Lava
294.8 Km²
Oldest Lava
353.7 Km²
Spectral Profile
Value
Band Number
1.1×10⁴
1.0×10⁴
9.0×10³
8.0×10³
7.0×10³
2
3
4
5
6
7

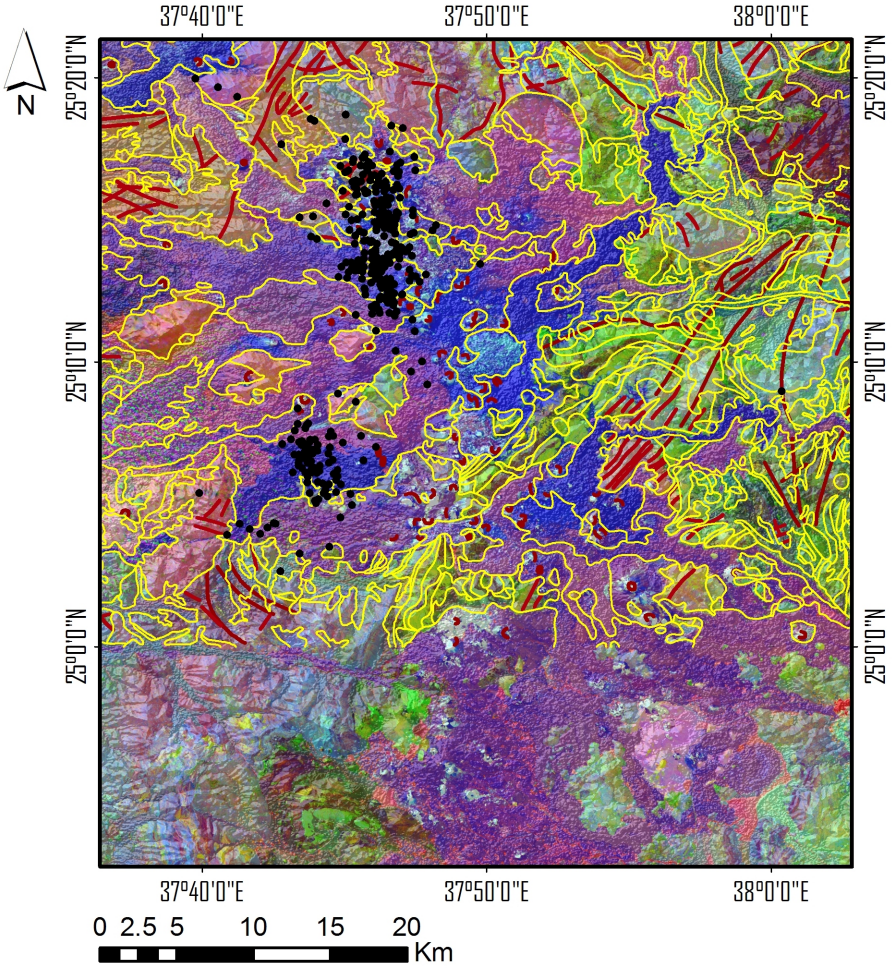
37°40'0"E
37°50'0"E
38°0'0"E
25°20'0"N
25°10'0"N
25°0'0"N
N
0 2.5 5 10 15 20
Km